Available online at www.sciencedirect.com
SCIENCE DIRECT
Cement and Concrete Research 36 (2006) 1091 – 1097
Cement and Concrete Research

Euclidean Distance Mapping for computing microstructural gradients at interfaces in composite materials

H.S. Wong *, N.R. Buenfeld

Concrete Durability Group, Department of Civil and Environmental Engineering, Imperial College London, SW7 2AZ, UK

Received 20 April 2005; accepted 9 October 2005

Abstract

This paper presents an image analysis procedure using Euclidean Distance Mapping to compute microstructural gradients at interfaces in composite materials. This method is capable of producing phase distribution plots at single pixel strip width very quickly and efficiently. Compared to conventional dilation–subtraction strip analysis, the new method is faster, more flexible and is not constrained by feature geometry and boundary conditions. This allows for truly random and unbiased sampling. The new method was applied to investigate microstructural gradients at the interfacial transition zone (ITZ) of an ordinary Portland cement concrete. The average results show strong gradients in anhydrous cement and detectable porosity at the ITZ, but this is highly variable from location to location. The overall ITZ characteristics depend on the amount of calcium hydroxide deposited on aggregate particles. The new method was able to measure the effect of these calcium hydroxide deposits on the porosity gradient, which has not been reported before.

Keywords: Backscattered electron imaging; Image analysis; Interfacial transition zone; Microstructure; Euclidean distance map

1. Introduction

Interfaces influence the bulk properties and overall performance of composite materials. In hardened concrete, interfaces exist between cement paste and steel reinforcement, fibres and also between the various phases within the cement paste itself. An important interface is the paste region adjacent to aggregate particles, known as the interfacial transition zone (ITZ); this is often regarded as the 'weakest link' that controls mechanical strength and is suspected to be detrimental to most aspects of the durability of concrete.

Researchers have used image analysis on backscattered electron (BSE) images to investigate and quantify microstructural gradients across the ITZ. This procedure, pioneered by Scrivener and co-workers [1–3], measures the distribution of phases, typically pores, anhydrous cement and calcium hydroxide, from the aggregate boundary. This is done by computing the area fractions of each phase in a series of narrow and equidistant strips or bands, starting from the interface and extending outward to the bulk paste. The relative fraction of each phase is averaged over a large number of images taken from different aggregate particles and the results plotted against distance from the aggregate surface.

The typical image analysis routine for quantitative phase analysis via a series of equidistant strips from the interface is briefly described here. The phase of interest, for example pores, is segmented from the BSE image by greyscale thresholding. A binary aggregate mask is also generated, usually by manually tracing the aggregate boundary. The binary aggregate mask is then dilated for a number of iterations depending on the pixel spacing and width of the strip to be created. The original aggregate mask is subtracted from the dilated image to give the first strip and a logical operation AND between the strip and pore mask is performed to give the fraction of pores located in the strip. To generate the subsequent strip and phase fraction, the aggregate mask is dilated again and the whole process is repeated.

The dilation–subtraction method requires significant processing time and computer memory due to the iterative nature and large number of images involved. For each strip, three images have to be created: the dilated boundary mask, the strip and the phase fraction contained within the strip. Additional

* Corresponding author. Tel.: +44 20 7594 5957; fax: +44 20 7225 2716.
E-mail address: hong.wong@imperial.ac.uk (H.S. Wong).

0008-8846/$ - see front matter © 2005 Elsevier Ltd. All rights reserved.
doi:10.1016/j.cemconres.2005.10.003

steps are the area measurements of the strip and pores contained within it. A typical ITZ analysis of 50 frames at a 2.5 μm strip width up to a distance of 50 μm from the aggregate will require 20 strips per interface, hence involving 60 images per frame and 3000 images for the complete analysis. If a different strip width is needed, then the whole process would have to be repeated. Investigation using a greater number of frames in smaller bands enables phase distribution to be analysed in greater detail, but narrower strips are impractical. Another disadvantage of the strip method is that special care has to be taken so that the strips are not generated beyond mid-distance to the next aggregate. To implement this into an automated image analysis algorithm is difficult because a randomly selected area in a typical concrete may contain aggregates separated at a distance of several microns to hundreds of microns. The strips may be generated manually, but this is extremely laborious and impractical. Thus, the operator is resigned to only selectively analyse paste areas where the distances between aggregate particles are large, but these results are not representative because of biased sampling.

In this paper, an alternative approach to interfacial analysis using Euclidean Distance Mapping (EDM) is proposed. The new method is more efficient as it does not involve a repetitive strip producing stage. The method only involves two additional images per location in order to obtain a gradient plot at a single pixel resolution, i.e., at one pixel wide strips. It is also more flexible than the conventional strip method because the information obtained from the EDM is sufficient to generate distribution plots at any strip width without requiring additional images. The new method is also applicable to any paste

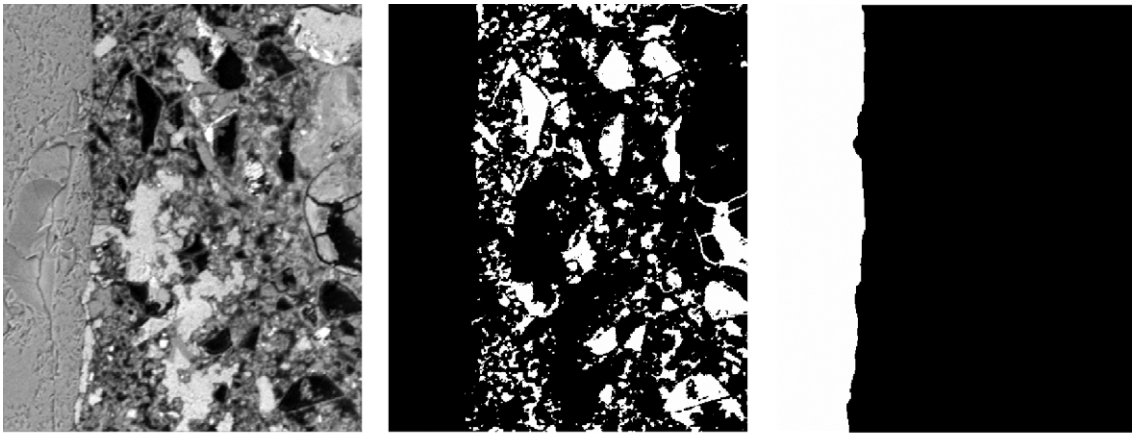

a) BSE image of a paste region adjacent to an aggregate particle. Field of view: 100 x 120μm

b) Pore binary mask.

c) Aggregate binary mask

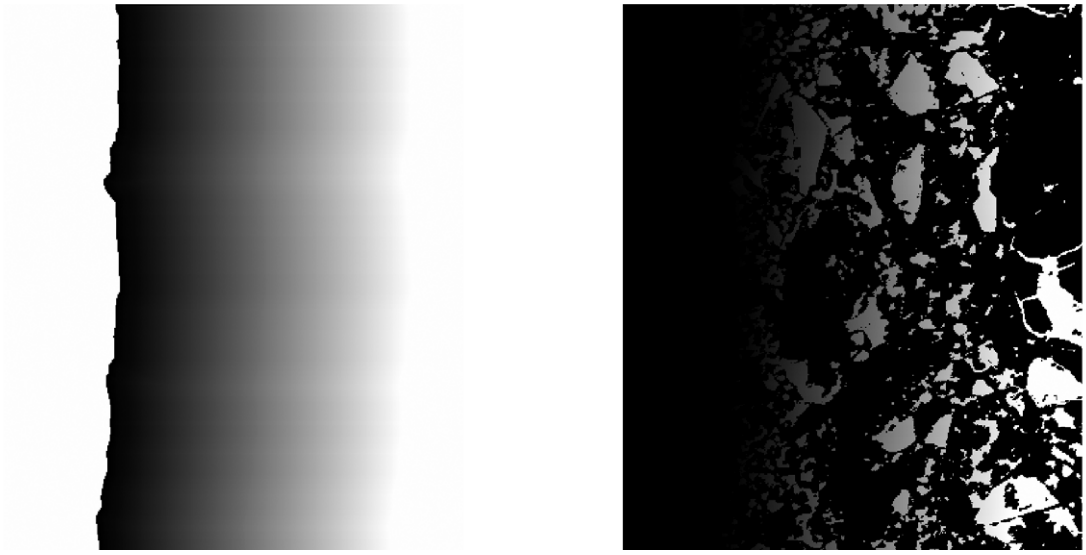

d) EDM of paste from the aggregate boundary. The grey value of each pixel in the paste increases with its nearest distance from the boundary.

e) Distance map of the pore phase from the aggregate boundary. The brightness of each pore pixel represents its nearest distance to the aggregate.

Fig. 1. Generating a Euclidean Distance Map (EDM) of the pore phase from the aggregate boundary.

geometries and boundary conditions. This paper presents applications of the new method to investigate microstructural gradients at the ITZ, emphasising that the same technique can be used for any type of interphase boundary.

2. Euclidean Distance Mapping for phase analysis

Euclidean Distance Mapping (EDM) is a basic operation used in computer vision, pattern recognition and robotics [4], where high speed computation is essential. It uses distance transformation to convert a binary image consisting of foreground and background pixels into a greyscale image where each pixel has a brightness value equal to its Euclidean (linear) distance to the nearest background pixel [5,6]. This can be expressed mathematically as follows. Consider a digital image $M=\{m_{ij}\}$ consisting of an array of $N\times M$ unit square pixels. The element in the ith row and jth column is denoted by (i, j). A binary image of M is defined by $B=\{b_{i,j}\}$ where each pixel element $b_{ij}\in\{0, 1\}$, 0 represents black (or background) and 1 represents white (or feature). The Euclidean Distance Mapping $D=\{d_{i,j}\}$ of the binary image $B=\{b_{i,j}\}$ is defined by:

$$d_{i,j}=\min_{p\geq 1,q\leq N}\left\langle\sqrt{(i-p)^2+(j-q)^2}\,|\,b_{pq}=0\right\rangle,\ \text{for all } i,j.$$

Since its introduction by Danielsson [4], many algorithms have been proposed for generating an efficient, fast and error-free EDM. Examples of applications are segmenting touching and overlapping features (watershed segmentation), computing fractal dimension and skeletonisation [6]. The EDM function is now available in almost all commercial image processing software packages. The EDM is advantageous because it is more isotropic and avoids directional bias that is present in pixel-by-pixel morphological operations such as erosion and dilation. The distance map can be constructed quickly and does not require iteration, so the run time does not increase with feature size [6].

Fig. 1 shows how EDM is applied for phase analysis at interfaces using a BSE image of the paste region adjacent to an

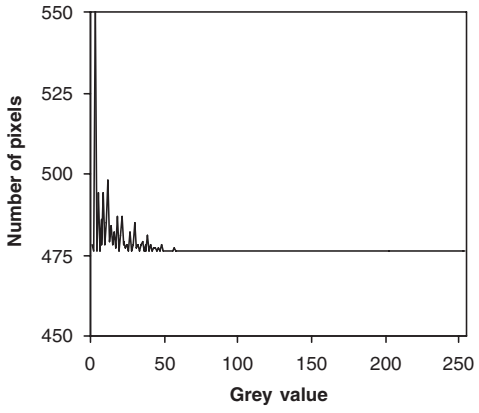

a) Brightness histogram of Fig. 1(d). The grey value 255 (white) representing aggregate is not plotted.

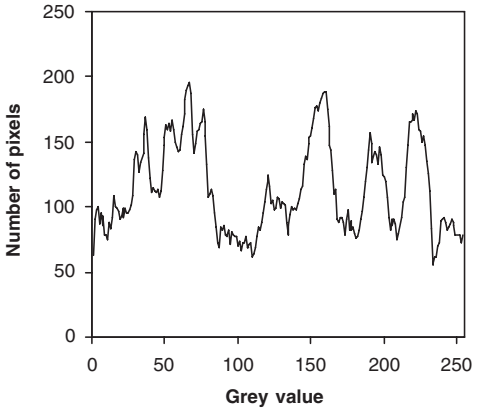

b) Brightness histogram of Fig. 1(e). The grey value 0 (black) representing the solid phase is not plotted.

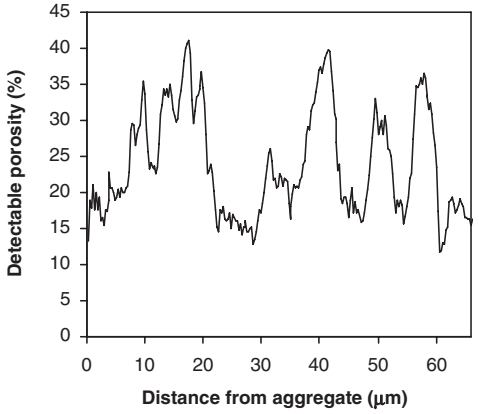

c) Porosity distribution from interface at 1pixel (0.26μm) strip width.

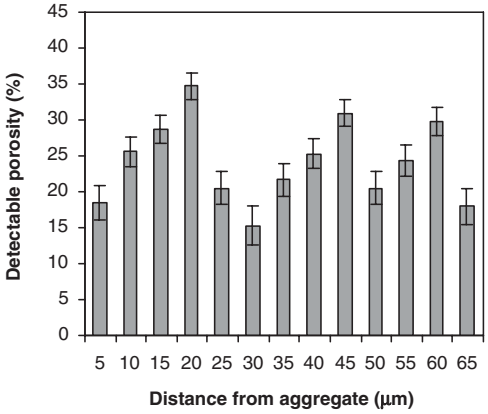

d) Porosity distribution from interface at 5μm strip width resolution. The y-error bars represent relative standard error ($1/\sqrt{N}$),where N is the number of pore pixels counted.

Fig. 2. Use of EDM for quantitative phase analysis at the aggregate–paste interface.

aggregate particle (Fig. 1a) as an example. To determine the porosity gradient from the aggregate boundary, first, the binary mask of the pore (Fig. 1b) and aggregate (Fig. 1c) phase is created. Next, an EDM of the paste (Fig. 1d) is generated from the aggregate binary mask. Then, a multiplicative operation is performed between the paste EDM and the pore mask, giving an EDM of the pore phase only (Fig. 1e). Observe that each pore pixel in the original binary image is now transformed to a grey value that has a numerical value equal to its linear distance to the nearest aggregate pixel, i.e., a particular pore pixel with grey value of x is located x pixels away from the nearest aggregate boundary.

Next, the brightness histogram of the paste and pore EDM are plotted in Fig. 2a and b, respectively. Normalising the brightness histogram of the pore EDM to the paste EDM, and converting the grey values to actual distances by factoring with the pixel spacing give the porosity distribution from the interface at a single pixel step (Fig. 2c). From this data, the porosity distribution can be re-plotted at any strip width, if desired. Fig. 2d gives an example where the porosity gradient is re-plotted at 5 μm intervals.

Another advantage of the new method is that it is easily applied on any geometry and boundary conditions. A BSE image of an OPC concrete is shown in Fig. 3a. Note the random nature of the paste and the range of separation distances between aggregates. As mentioned earlier, unless the strips are generated manually, the conventional dilation–subtraction strip method can only be applied where the separation distance between adjacent boundaries are at least twice the distance to the furthest strip, typically around 50 μm. Therefore, for the example in Fig. 3a, only the lower half of the image is suitable for strip analysis. This can create biased sampling and non-representative results, no matter how many images are averaged. Fig. 3b–d shows that the new method is applicable to any paste geometry easily, thus all areas are included. Note that there is an uncertainty in the distance map for features near the image border because influences from aggregate particles outside the image have not been accounted

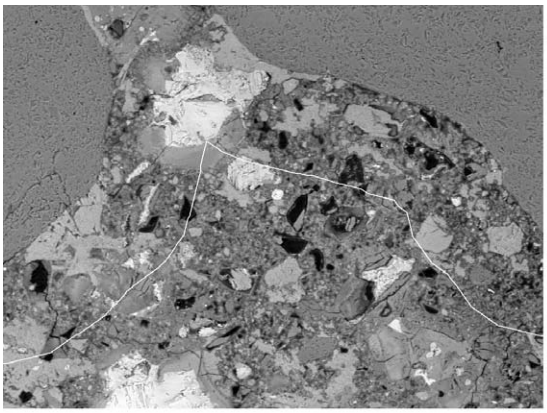

a) Concrete (w/c 0.5). The white border represents the 50μm strip. Field of view: 267 x 200μm

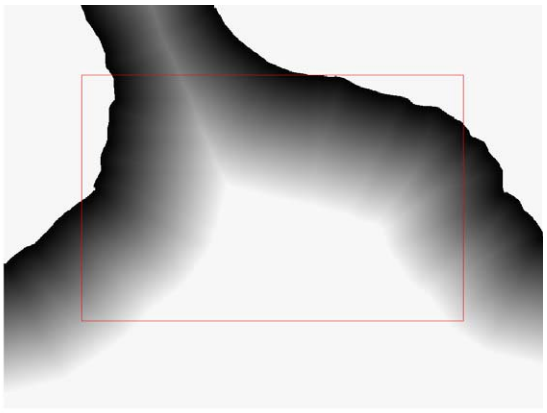

b) EDM of paste from aggregate boundary. The phase analysis is confined to features located 50μm from the edge of the image, i.e. contained in the box.

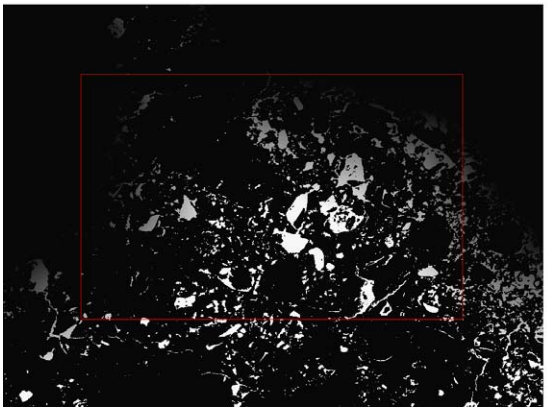

c) Distance map of pores.

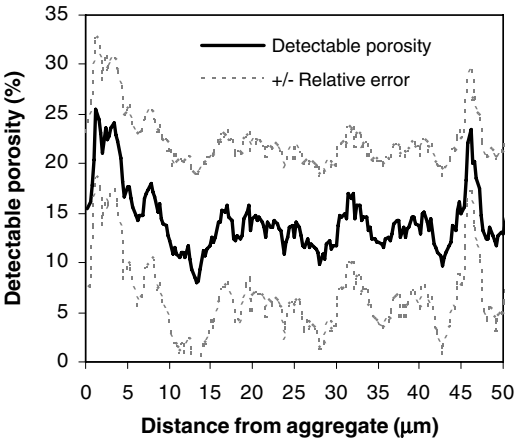

d) Porosity distribution from interface at 1 pixel (0.26μm) strip width.

Fig. 3. Applying the EDM method on a random section of an OPC concrete. The porosity distribution from the aggregate–paste interface is obtained by normalising the brightness histogram of the pore EDM to the brightness histogram of the paste EDM.

for. Therefore, in Fig. 3b and c, the distance maps are cropped by an amount equal to the distance of the furthest 'strip', in this case 50 μm.

3. Example of application

In this section, the new method will be used to investigate spatial distribution of detectable porosity and anhydrous cement at the ITZ. For this purpose, an OPC concrete at water–cement ratio 0.4 was prepared. A cylindrical sample (100 $\Phi \times 250$ mm) was cast, demoulded after 24 h and wrapped in cling film for 3 days. After curing, an 8 mm thick disc was cut from approximately 100 mm from the bottom cast face, from which a block sample (40×20 mm) was sectioned. The block was freeze-dried, vacuum-impregnated with a low viscosity epoxy, ground and polished using successively finer grit size down to 1/4 μm. To ensure a deep epoxy penetration, the vacuum-impregnated sample was pressurised at 2.5 bar above atmosphere for 30 min [7]. A non-aqueous solution was used as lubricant for cutting and polishing. Acetone was used as cleaning fluid.

A JEOL 5410LV scanning electron microscope, operated at low vacuum (9 Pa), 10 kV accelerating voltage and 10 mm free working distance was used for imaging. Thirty images (1024×768 pixels, pixel spacing 0.26 μm) were captured at 500× magnification. In order to minimise risk of local variation, the sampling procedure should obtain many images taken at different locations, dispersed over a large area and different aggregate particles. Thus, a uniform random sampling procedure was adopted. The microscope stage was programmed to move in a grid, stopping at thirty predefined, equally spaced coordinates spanning the entire sample. If a frame fell entirely on an aggregate particle or entirely on paste, it was replaced by another location within the neighbouring grids, chosen from a random number table.

Each image was captured with a constant brightness and contrast settings for reproducibility. The brightness and contrast were calibrated with an aluminium-epoxy microanalytical standard so that the image greyscale histogram was stretched to cover the entire greyscale, but not over-saturated at the low and high ends of the spectrum. The pore phase was segmented using the 'overflow' method [8]; the inflection point of the cumulative brightness histogram was taken as the upper threshold grey value for pores. The anhydrous cement phase was segmented by using the minimum point between the peaks for hydrated paste and anhydrous phase as the lower threshold value. Bond cracks appearing at the interface and air voids were excluded from the analysis. We have decided not to analyse the calcium hydroxide (CH) phase due to problems in segmentation. The grey values for CH and other hydrated phases tend to overlap significantly and it is very difficult to confidently isolate these on the basis of grey value alone. As mentioned by Scrivener et al. [2], the distance measured on a random plane section will overestimate the true normal distance from the aggregate surface. In this work, no attempt was made to correct for this effect and all distances are reported as measured.

Fig. 4 shows the distribution of anhydrous cement particles and detectable porosity from the aggregate–paste interface at one pixel strip width. Results are expressed as area percentage of the cement paste. Fig. 4a clearly shows a deficit in cement grains near the boundary compared to bulk paste. The very pronounced anhydrous cement gradient is due to disrupted packing of cement grains against much larger aggregate particles, i.e. the 'wall-effect', which is generally regarded as the basis of the ITZ phenomena. The anhydrous cement fraction increased steadily from 1% at the boundary to around 14% at 50 μm away. However, the distribution of detectable porosity from the interface, shown in Fig. 4(b), gave interesting results. At less than 5 μm away from the interface, there appears to be a sudden drop in detectable porosity, giving an impression that the aggregates are surrounded by a thin layer of paste that is almost as dense as the bulk paste. We note that this feature has not been reported before, possibly because previous studies were at lower resolution. Nevertheless, the general trend is conventional; porosity decreases with increasing distance from the interface and the value at the boundary is approximately twice that of the bulk region. From Fig. 4, it appears that the ITZ extends to around 50 μm away from the aggregate surface, with respect to both anhydrous cement and detectable porosity gradients.

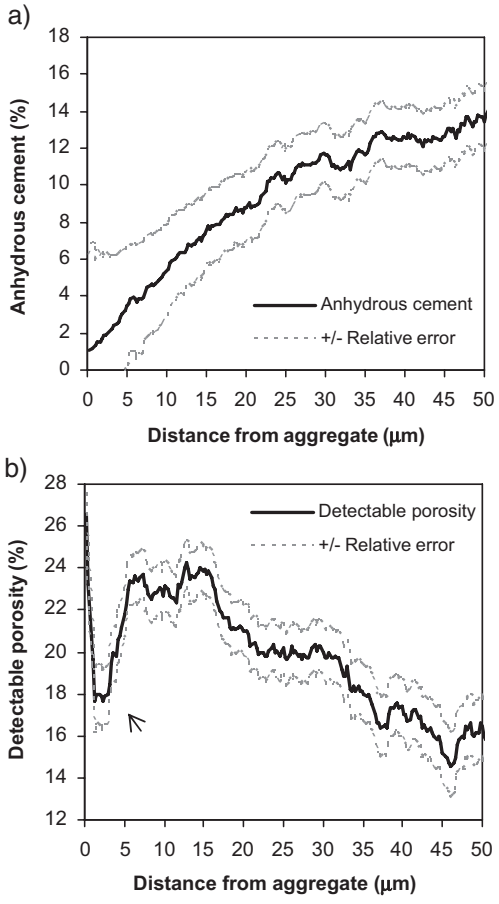

Fig. 4. Detectable anhydrous cement (a) and porosity distribution (b) plots at single pixel strip width, measured from the aggregate–paste interface. Values are the average of 30 frames.

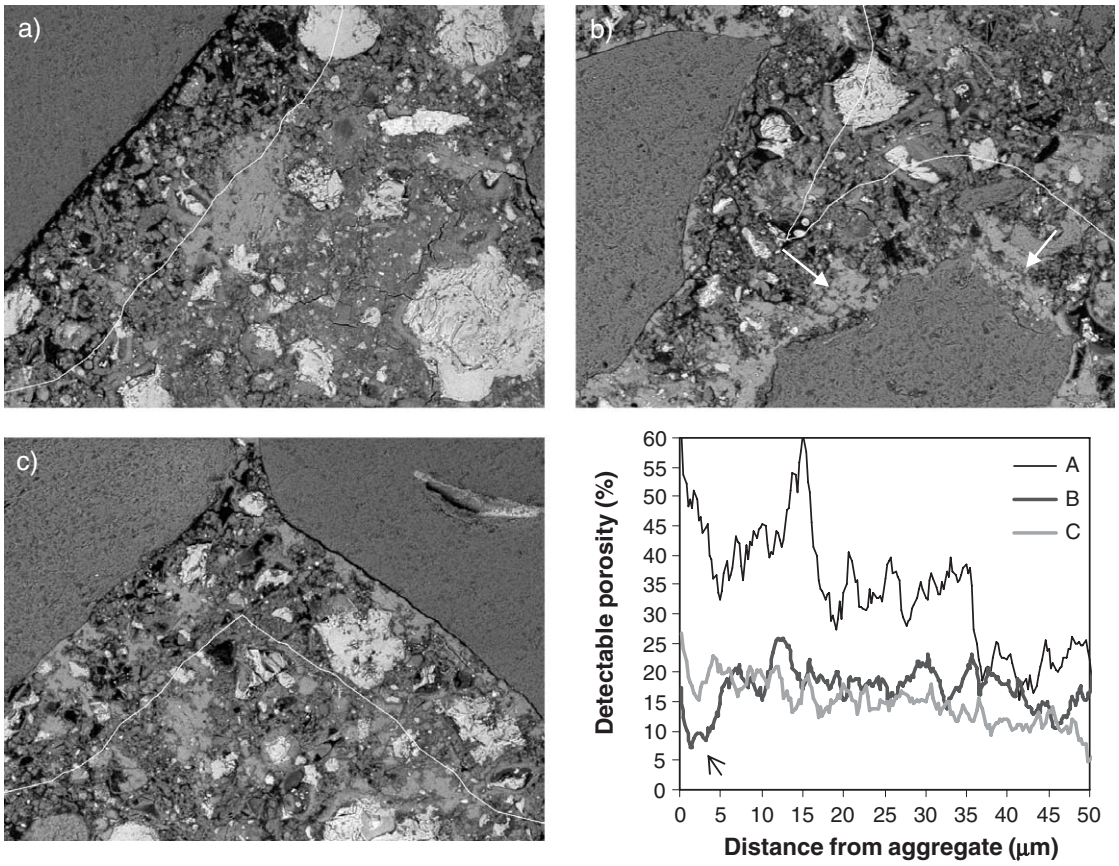

Fig. 5. Detectable porosity distribution plots showing different ITZ characteristics: A) very porous ITZ; B) relatively dense ITZ with large amount of CH deposits on the aggregate surface (arrowed); and C) mixture of porous and dense ITZs. The averaged result will depend on the relative proportion of the porous and dense ITZ. Note that the bond cracks visible in A and C are not tallied. White border represents the 50 μm strip (field of view: 267 × 200 μm).

After a thorough check on all the images and individual porosity gradients, we observed three types of ITZ characteristics, shown in Fig. 5. The first appears to be a very porous ITZ, with a strong porosity gradient, the detectable porosity at the interface almost three times that of the bulk paste. This may be similar to the ITZs originally reported by Scrivener et al. [1,2]. The second is much denser with large amounts of CH deposited on the aggregate surface. The detectable porosity gradient is weak and there is a sudden drop in porosity at less than 5 μm from the aggregate surface due to the presence of CH. This may be similar to that reported by Diamond and Huang [9,10]. The third type contains a mixture of 'porous' and 'dense' ITZs; the porosity gradient is evident, but is not as strong as the first example. Obviously, the 'average' porosity gradient of the ITZ will depend on the relative proportion of the 'porous' and 'dense' ITZs contained in the sample set. However, the presence, size and shape of CH deposits are very irregular; we observed that some aggregate particles are almost completely lined with CH in the 2D observation plane, while others are entirely free of it. Therefore, the sampling method will also have an influence on the measured 'average' porosity gradient. For example, results obtained from studies that adopt a uniform random sampling method, e.g., Scrivener et al. [1, 2] will be different from those that select an aggregate particle and then capture a succession of adjacent images around the chosen grain, e.g., Diamond and Huang [9,10]. This could be the reason why in the study by Diamond and Huang [10], high porosity was not observed within the first 5 μm of the aggregate surface.

Another important issue is the degree of variability in the observed microstructural gradients at different locations. Although the deficiency in anhydrous cement and excess in detectable porosity at the ITZ is evident and clearly seen in the averaged results, there is however, a significant variability from

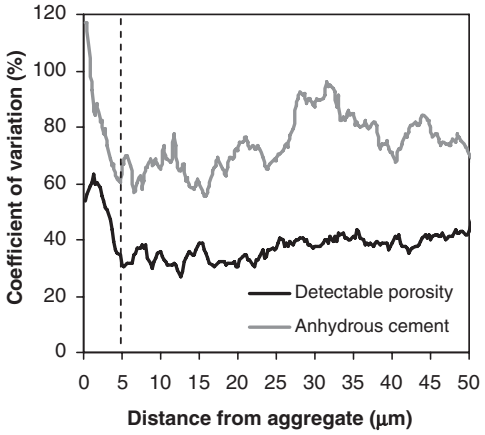

Fig. 6. Coefficients of variation for the average detectable porosity and anhydrous cement plotted against distance from aggregate surface. Note the high variability, particularly at less than 5 μm from the aggregate surface.

location to location. Fig. 6 shows the coefficient of variation for the mean anhydrous cement and detectable porosity, plotted against distance from the aggregate surface. The coefficient of variation ranges between 30% and 60% for detectable porosity and between 60% and 120% for anhydrous cement. It is noted that the variability is particularly high in the first 5 μm from the aggregate surface and this is likely to be due to the variability in the amount of CH deposited on aggregate particles. We also note that the size of the 'CH influence zone' as observed in Fig. 6 matches that of the one in the porosity gradient (Fig. 4b). However, it is stressed that the number of samples investigated in this study is limited and the results are preliminary. Nevertheless, the high variability in the microstructural gradients is real and as emphasised by Diamond and Huang [9,10], must be given consideration in computer models that attempt to simulate the microstructure of cement-based materials.

4. Conclusion

A new image analysis method for investigating microstructural gradients at interfaces in composite materials is presented. The method uses Euclidean Distance Mapping to generate microstructural gradient plots at single pixel strip width. The new method is faster and more flexible than conventional dilation–subtraction strip analysis, and is not constrained by feature geometry and boundary conditions. Therefore a truly random and unbiased sampling procedure can be achieved. The new method was applied to investigate microstructural gradients at the interfacial transition zone of an ordinary Portland cement concrete sample. The results showed that although the overall ITZ can be characterised by a strong gradient in anhydrous cement and detectable porosity, this is highly variable from location to location. The higher sensitivity of the new method enabled it to detect previously unreported effects of calcium hydroxide deposits on the aggregate surface on the porosity gradient. The measured 'average' characteristic of the ITZ via image analysis is dependent upon the extent of CH deposition at aggregate surfaces and also on the adopted sampling procedure.

Acknowledgements

HSW would like to acknowledge the financial assistance provided by the Universities of UK, via the Overseas Research Students Awards Scheme. We thank Mr. R. A. Baxter for his help with the laboratory work.

References

[1] K.L. Scrivener, E.M. Gartner, Mater. Res. Soc. Symp. Proc. 114 (1988) 77.
[2] K.L. Scrivener, A.K. Crumbie, P.L. Pratt, Mater. Res. Soc. Symp. Proc. 144 (1988) 87.
[3] K.L. Scrivener, A. Bentur, P.L. Pratt, Adv. Cem. Res. 1 (4) (1988) 230.
[4] P.E. Danielsson, Comp. Graph. Image Process. 14 (1980) 227.
[5] A. Rosenfeld, J. Pfaltz, Pattern Recogn. 1 (1968) 33.
[6] J.C. Russ, The Image Processing Handbook, Fourth edition, CRC Press, London, 2002, 744 pp.
[7] H.S. Wong, N.R. Buenfeld. Patch microstructure in cement-based materials: fact or artefact? Cem. Concr. Res. (in press).
[8] H.S. Wong, M.K. Head, N.R. Buenfeld, Pore segmentation of cement-based materials from backscattered electron images, Cem. Concr. Res. 36 (2006) 1083–1090.
[9] S. Diamond, J. Huang, in: A. Katz, A. Bentur, M. Alexander, G. Arliguie (Eds.), Proc. RILEM 2nd Int. Conf. On the Interfacial Transition Zone in Cementitious Composites, vol. 35, RILEM Publications SARL, Paris, 1998, p. 1.
[10] S. Diamond, J. Huang, Cem. Concr. Compos. 23 (2001) 179.